Towards Reliable and Interference-Aware CSI Feedback with Bayesian Neural Network

Ifiok Udoidiok, Bruno Fonkeng, Jielun Zhang, and Fuhao Li
School of Electrical Engineering & Computer Science, University of North Dakota, Grand Forks, ND, 58202, USA
{ifiok.udoidiok, bruno.fonkeng, jielun.zhang, fuhao.li}@UND.edu

***Abstract*—Channel state information feedback is essential for efficient communication between user equipment and base stations in wireless networks. Deep learning-based channel state information feedback models have shown great potential in compressing and reconstructing channel state information matrix, significantly reducing communication overhead. However, these models often assume ideal transmission conditions and overlook the challenges posed by interference, which can affect the reliability of feedback and reconstruction. To address these issues, we propose a Bayesian Neural Network based framework for reliable and interference-aware channel state information feedback. In specific, the proposed framework not only compresses and reconstructs channel state information but also incorporates uncertainty estimation to detect potential interference during transmission. Experimental results demonstrate that the proposed framework ensures high-quality channel state information reconstruction while promptly detecting and responding to interference, thereby enhancing the reliability of the feedback.**

***Index Terms*—Channel state information feedback, Bayesian neural networks, Uncertainty estimation, Interference detection, Deep learning.**

I. Introduction

Channel State Information (CSI) feedback is fundamental for wireless communication systems, facilitating efficient communication between User Equipment (UE) and Base Stations (BS) [1], [2]. Accurate CSI feedback supports critical operations, including resource allocation, beamforming, and interference management, ensuring optimal system performance [3]. Traditional methods, such as Singular Value Decomposition (SVD) and quantization techniques, have been widely used to compress CSI and reduce feedback overhead [4]. However, these methods often fail to capture the intricate spatial and temporal correlations inherent in modern wireless channels, which are critical for maintaining reliable performance in diverse and dynamic environments [5].

With the advent of deep learning, CSI feedback has witnessed a significant paradigm shift, achieving superior performance compared to traditional approaches [6]–[8]. Deep learning models leverage neural networks to automatically extract complex spatial and temporal features from CSI data, significantly improving compression efficiency and reconstruction accuracy. For example, The authors in [6] proposed CsiNet, which a Convolutional Neural Network (CNN)-based model that effectively captures spatial correlations within CSI matrices, achieving high compression ratios while maintaining low reconstruction error. Similarly, The authors in [7] proposed CsiNet+ as an advanced variant of CsiNet, which serves as a compressive sensing neural network framework that incorporates multi-rate quantization strategies and parameter visualization to address the CSI feedback problem. The method improves reconstruction accuracy and reduces storage requirements at the user equipment. The authors in [8] introduced a CQNet, a DL-based framework that optimizes CSI compression and recovery by incorporating magnitude-adaptive phase quantization. It achieves higher compression efficiency and better reconstruction accuracy compared to traditional methods, making it well-suited for bandwidth-constrained massive MIMO systems. These advancements underscore the potential of deep learning to address the limitations of traditional methods. However, most existing models operate under the assumption of ideal transmission conditions, ignoring real-world challenges such as interference, noise, and varying channel conditions [9]. In particular, intentional interference, such as maliciously injected noise, can significantly distort the transmitted data, leading to severe degradation in the quality of the reconstructed CSI and potentially causing substantial errors in downstream tasks like beamforming and resource allocation.

To address these challenges, we propose a Bayesian Neural Network (BNN)-based CSI feedback framework that incorporates uncertainty estimation and interference detection. The proposed framework can effectively compresses and reconstructs CSI while quantifying uncertainty in the predictions to detect potential interference during transmission. To be specific, the model performs multiple stochastic predictions on the received CSI data and calculates the variance of outputs to measure uncertainty. When the uncertainty exceeds a predefined threshold, the system identifies the presence of interference and triggers appropriate actions, such as notifying the UE for retransmission or adjusting the reconstruction process to mitigate the effects of interference. In this case, the proposed framework ensures reliable CSI feedback and robust reconstruction under challenging transmission conditions. The proposed framework is evaluated using dataset generated from the COST 2100 channel model [10]. Experimental results demonstrate that the framework maintains high reconstruction quality while detecting interference in the feedback data. The main contributions of this work are as follows: 1) We proposed a CSI feedback framework based on Bayesian Neural Networks, which incorporates uncertainty estimation to support CSI reconstruction. 2) We developed a mechanism

to detect interference during CSI transmission by analyzing prediction variance and applying an uncertainty threshold. 3) We evaluated the proposed framework on benchmark datasets, demonstrating its capability to detect interference and maintain reconstruction accuracy under various conditions.

The rest of this paper is organized as follows. Section II describes the system and the problem. Section III introduces the proposed framework for CSI reconstruction and interference detection. Section IV demonstrates the evaluation results. Section V concludes the paper and introduces future research directions.

II. System Description and Problem Statement

A. System Description

We consider a Multiple-Input Multiple-Output (MIMO) communication system consisting of a BS with N_t antennas and a UE with a single receive antenna. The system operates in an orthogonal Frequency Division Multiplexing framework with N_c subcarriers. The received signal at the n-th subcarrier can be modeled as:

$$y_n = \mathbf{h}_n^H \mathbf{v}_n x_n + z_n, \tag{1}$$

where $\mathbf{h}_n \in \mathbb{C}^{N_t \times 1}$ is the channel vector, $\mathbf{v}_n \in \mathbb{C}^{N_t \times 1}$ is the precoding vector, $x_n \in \mathbb{C}$ is the transmitted symbol, and $z_n \in \mathbb{C}$ represents additive white Gaussian noise. The full CSI matrix $\mathbf{H} = [\mathbf{h}_1, \mathbf{h}_2, \ldots, \mathbf{h}_{N_c}]^H \in \mathbb{C}^{N_c \times N_t}$ is critical for enabling effective beamforming, precoding, and resource allocation at the BS [11]. However, transmitting the full-resolution CSI matrix from the UE to the BS in Frequency Division Duplex (FDD) systems is impractical due to limited feedback bandwidth. To address this, the UE compresses $\mathbf{H}$ into a low-dimensional representation $\mathbf{X}$, which is then transmitted to the BS through feedback links.

B. Problem Statement

In the CSI feedback process, the compressed CSI $\mathbf{X}$ transmitted from the UE to the BS is often subject to noise and interference in the feedback channel [12]. These interferences may include typical random noise or unintended disturbances caused by environmental factors or hardware issues. Additionally, in certain scenarios, the feedback channel may be subjected to deliberate interference, such as malicious signal injection, further compromising the integrity of the transmitted data. As a result, the received feedback data at the BS can be expressed as:

$$\mathbf{X}_{\text{rec}} = \mathbf{X} + \mathbf{N}, \tag{2}$$

where $\mathbf{N}$ represents the combined effects of noise, unintended interference, and potential deliberate interference. Such distortions not only degrade the quality of the reconstructed CSI matrix $\hat{\mathbf{H}}$ but can also significantly impair communication performance. Existing deep learning-based CSI feedback models typically assume ideal transmission conditions and fail to account for the presence of various types of interference or noise in the feedback channel. However, such disturbances are inevitable in real-world systems with deliberate interference adding an additional layer of uncertainty to the system. Therefore, it is crucial to detect whether the received feedback data $\mathbf{X}_{\text{rec}}$ has been corrupted, particularly in cases where malicious interference might be present. To address this issue, this paper focuses on interference detection in the compressed CSI feedback process and proposes a Bayesian Convolutional Neural Network (BCNN) to estimate uncertainty in the reconstruction process. By analyzing the variance of predictions generated by the BCNN, the system can identify feedback data corrupted by various interferences, including deliberate interference, without relying on explicit signal-level information. This approach provides a robust and efficient mechanism to detect interference and enhance the reliability of the CSI feedback process, addressing the challenges posed by complex and unpredictable real-world communication environments.

III. The Proposed Framework for CSI feedback model with inference detection

A. Overview of the Proposed Framework

The proposed CSI feedback framework combines deep learning-based compression with Bayesian learning to enhance reliability in wireless communication. The framework consists of an encoder at the UE side and a Bayesian decoder at the BS side. The encoder compresses high-dimensional CSI matrices into compact codewords, effectively reducing feedback overhead. The encoder compresses high-dimensional CSI matrices into compact codewords, effectively reducing feedback overhead. At the Base Station (BS), the Bayesian decoder simultaneously reconstructs the CSI matrix and performs interference detection. Specifically, the decoder calculates an uncertainty score by generating multiple stochastic reconstruction results and evaluates potential interference based on the variance of these results. If the uncertainty score exceeds a predefined threshold, the system identifies possible interference and triggers corrective actions, such as retransmissions or reconstruction adjustments. If the data is normal, the average of the multiple reconstruction results is used as the final reconstructed CSI matrix. The details of the encoder-decoder design and the uncertainty-based detection mechanism are explained in the following subsections.

B. DL-based CSI Feedback Model with Bayesian Learning

The proposed CSI feedback model is based on the encoder-decoder architecture of CsiNet+ [7], enabling efficient compression and reconstruction of CSI while incorporating Bayesian learning in the decoder for enable the interference detection. For an input CSI matrix $\mathbf{H}$, the encoder extracts spatial features through convolutional layers and maps these features into a low-dimensional compact codeword $\mathbf{X}$:

$$\mathbf{X} = f_{\text{enc}}(\mathbf{H}; \mathbf{W}_{\text{enc}}), \tag{3}$$

where f_{enc} represents the encoder function, and $\mathbf{W}_{\text{enc}}$ denotes its parameters. The generated codeword $\mathbf{X}$ is a compressed representation of $\mathbf{H}$. The codeword $\mathbf{X}$ is then transmitted to the BS through the feedback link.

At the BS, the decoder reconstructs the CSI matrix $\hat{\mathbf{H}}$ from the received codeword $\mathbf{X}_{\text{rec}}$ using Bayesian learning [13], [14]. The relationship between the input $\mathbf{X}_{\text{rec}}$ and the reconstructed output $\hat{\mathbf{H}}$ can be denoted as:

$$p(\hat{\mathbf{H}}|\mathbf{X}_{\text{rec}}, \mathcal{D}) = \int p(\hat{\mathbf{H}}|\mathbf{X}_{\text{rec}}, \boldsymbol{\theta}) p(\boldsymbol{\theta}|\mathcal{D})\, d\boldsymbol{\theta}, \tag{4}$$

where $\boldsymbol{\theta}$ represents the model parameters, and $\mathcal{D}$ denotes the training dataset. Since directly computing this integral is intractable, an approximate posterior distribution $q(\boldsymbol{\theta}|\mathcal{D})$ is employed. The optimization objective minimizes the Kullback-Leibler (KL) divergence between the approximate posterior $q(\boldsymbol{\theta}|\mathcal{D})$ and the true posterior $p(\boldsymbol{\theta}|\mathcal{D})$:

$$D_{\text{KL}}(q(\boldsymbol{\theta}|\mathcal{D}) \| p(\boldsymbol{\theta}|\mathcal{D})) = \int q(\boldsymbol{\theta}|\mathcal{D}) \log \frac{q(\boldsymbol{\theta}|\mathcal{D})}{p(\boldsymbol{\theta}|\mathcal{D})}\, d\boldsymbol{\theta}. \tag{5}$$

To avoid direct computation of the KL divergence, variational inference is used to sample the weights $\boldsymbol{\theta}$ from $q(\boldsymbol{\theta}|\mathcal{D})$. The loss function is expressed as:

$$\begin{aligned} \mathcal{L}(\mathcal{D}, \boldsymbol{\theta}) = & \frac{1}{N} \sum_{n=1}^{N} \Big(\log q(\boldsymbol{\theta}^{(n)}|\mathcal{D}) \\ & - \log p(\boldsymbol{\theta}^{(n)}) - \log p(\mathbf{X}_{\text{rec}}|\boldsymbol{\theta}^{(n)}) \Big), \end{aligned} \tag{6}$$

where N is the number of samples drawn from the approximate posterior $q(\boldsymbol{\theta}|\mathcal{D})$. The decoder reconstructs the CSI matrix $\hat{\mathbf{H}}$ based on the optimal parameters $\boldsymbol{\theta}^*$ obtained during training:

$$\hat{\mathbf{H}} = f_{\text{dec}}(\mathbf{X}_{\text{rec}}; \boldsymbol{\theta}^*), \tag{7}$$

where f_{dec} represents the decoder function. The encoder and decoder are trained jointly using end-to-end learning. The training objective minimizes the mean squared error between the reconstructed CSI $\hat{\mathbf{H}}$ and the ground truth CSI $\mathbf{H}$:

$$\mathcal{L}(\Theta) = \frac{1}{T} \sum_{i=1}^{T} \| f_{\text{dec}}(f_{\text{enc}}(\mathbf{H}_i; \Theta_{\text{enc}}); \Theta_{\text{dec}}) - \mathbf{H}_i \|_2^2, \tag{8}$$

where $\Theta = \{\Theta_{\text{enc}}, \Theta_{\text{dec}}\}$ represents the parameters of the encoder and decoder, and T is the total number of training samples.

C. Uncertainty Score Estimation and Triggering Procedure

To enable the proposed CSI feedback model to reconstruct CSI matrices while analyzing whether the transmitted data has been corrupted, we introduce a variance-based uncertainty score. This method quantifies the stability of multiple stochastic reconstructions for the same data, providing an effective mechanism to evaluate the confidence in the received data.

In the Bayesian decoder, the received codeword $\mathbf{X}_{\text{rec}}$ is decoded into a series of stochastic CSI reconstructions by sampling the model parameters $\boldsymbol{\theta}$ from the approximate posterior distribution $q(\boldsymbol{\theta}|\mathcal{D})$. Specifically, the decoder generates M reconstructions, denoted as:

$$\hat{\mathbf{H}}^{(m)} = f_{\text{dec}}(\mathbf{X}_{\text{rec}}; \boldsymbol{\theta}^{(m)}), \quad m = 1, 2, \ldots, M,$$

where $\boldsymbol{\theta}^{(m)} \sim q(\boldsymbol{\theta}|\mathcal{D})$. The mean reconstruction matrix is then calculated as:

$$\mathbb{E}[\hat{\mathbf{H}}] = \frac{1}{M} \sum_{m=1}^{M} \hat{\mathbf{H}}^{(m)}.$$

Using the mean reconstruction, the uncertainty score U is defined as the variance among these stochastic reconstructions:

$$U = \frac{1}{M} \sum_{m=1}^{M} \left\| \hat{\mathbf{H}}^{(m)} - \mathbb{E}[\hat{\mathbf{H}}] \right\|_F^2,$$

where $\| \cdot \|_F^2$ represents the squared Frobenius norm. The uncertainty score U directly reflects the consistency of the reconstruction results. A low U indicates that the reconstructions are concentrated, suggesting high confidence in the reliability of the transmitted data. Conversely, a high U suggests significant dispersion among the reconstructions, which may result from interference or noise affecting $\mathbf{X}_{\text{rec}}$. After calculating the uncertainty score, it is compared against a predefined threshold τ. If $U > \tau$, the system determines that the data has been corrupted by interference and triggers remedial actions, such as requesting the UE to retransmit the data or employing robust optimization strategies to mitigate the impact of interference.

Algorithm 1 CSI Feedback Model with Bayesian Learning

Input : $\mathbf{H}$, M, τ, f_{enc}, f_{dec}
Output: $\hat{\mathbf{H}}$ or interference triggering
1. Compress the original CSI matrix $\mathbf{H}$ into a compact codeword $\mathbf{X}_{\text{rec}}$.
2. Transmit $\mathbf{X}_{\text{rec}}$ to the BS via the feedback link.
3. Initialize $\mathbb{E}[\hat{\mathbf{H}}] \leftarrow \mathbf{0}$, $U \leftarrow 0$, and $\{\hat{\mathbf{H}}^{(m)}\}_{m=1}^{M} \leftarrow \emptyset$.
4. **for** $m = 1$ *to* M **do**
   a) Sample parameters $\boldsymbol{\theta}^{(m)} \sim q(\boldsymbol{\theta}|\mathcal{D})$.
   b) $\hat{\mathbf{H}}^{(m)} = f_{\text{dec}}(\mathbf{X}_{\text{rec}}; \boldsymbol{\theta}^{(m)})$. // Reconstruct the CSI matrix.
   c) $\mathbb{E}[\hat{\mathbf{H}}] \leftarrow \mathbb{E}[\hat{\mathbf{H}}] + \frac{\hat{\mathbf{H}}^{(m)}}{M}$. // Update the mean reconstruction.
   d) Save $\hat{\mathbf{H}}^{(m)}$ into $\{\hat{\mathbf{H}}^{(m)}\}$.
end
5. **for** $m = 1$ *to* M **do**
   $D^{(m)} = \left\| \hat{\mathbf{H}}^{(m)} - \mathbb{E}[\hat{\mathbf{H}}] \right\|_F^2$.
   $U \leftarrow U + \frac{D^{(m)}}{M}$.
end
6. **if** $U > \tau$ **then**
   Declare interference detected and trigger corrective action.
   else
      $\hat{\mathbf{H}} = \mathbb{E}[\hat{\mathbf{H}}]$. // Output reconstructed CSI matrix.
   end
end

IV. Experiments

A. Dataset and Environment

The dataset used in this study follows the procedure outlined in [6]. It includes two types of channel matrices generated using the COST 2100 channel model, i.e., an indoor picocellular

scenario at the 5.3 GHz band and an outdoor rural scenario at the 300 MHz band. All parameters adhere to their default configurations as specified in the COST 2100 model [10]. In the indoor scenario, the BS is centrally located within a 20-meter square area, while in the outdoor scenario, the coverage extends to a 400-meter square area. UE is randomly distributed within these areas for each sample. The BS is equipped with a uniform linear array of 32 antennas and utilizes 1024 subcarriers. To optimize processing, the channel matrices are transformed into the angular-delay domain, retaining the first 32 rows, resulting in matrices of size 32×32. The dataset contains 100,000 training samples and 20,000 testing samples. The training set is further split into 80,000 samples for model training and 20,000 samples for validation during training. The testing dataset, consisting of 20,000 samples, is reserved for final performance evaluation.

To simulate real-world transmission environments, we introduced impulsive interference into the compressed latent feature data transmitted to the BS. Specifically, we used a parameter λ to denote the proportion of samples affected by interference and a parameter α to control the intensity of the interference, where α is expressed as a percentage of the maximum value of the transmitted data. By varying λ and α, different transmission conditions can be simulated. Simulation and evaluation of the proposed schemes are conducted on a workstation with an Intel® Core™ i7-14700K processor, 32 GB of RAM, a 4 TB SSD, and an NVIDIA GeForce RTX 4070 graphics card, using PyTorch 2.3.0 and Python 3.11.9 on Windows 11.

B. Model Initialization

To evaluate the proposed framework, we implemented the Bayesian CSI feedback model, named BCsiNet, and the baseline models CsiNet+ and CsiNet. The structure of the proposed BCsiNet is based on the Csinet+. The encoder consists of two convolutional layers with 7×7 kernels, padding of 3, and 2 input/output channels. These layers are followed by batch normalization and LeakyReLU activation functions. The features are then flattened and passed through a dense layer to produce a compressed codeword $\mathbf{X}_{\text{rec}}$. The decoder incorporates Bayesian learning, starting with a fully connected layer to decompress the codeword, followed by a Bayesian convolutional layer. It employs five RefineNet blocks with Bayesian convolutional layers of varying kernel sizes (7×7, 5×5, 3×3), batch normalization, and LeakyReLU activations. Residual connections are included in each block for stability and gradient flow. The reconstruction is finalized through a Bayesian convolutional layer with a Sigmoid activation, yielding the CSI matrix $\hat{\mathbf{H}}$.

CsiNet+ features a similar encoder-decoder structure, with 3×3 convolutional kernels and residual connections. The decoder uses convolutional layers for refinement with deterministic methods. CsiNet employs a simpler autoencoder design, with fewer convolutional layers and no advanced refinement or residual connections, making it less robust in challenging transmission scenarios. The epochs, initial learning rate, and batch size are set to 200, 0.001, and 64, respectively, with the learning rate reduced to 99% of its current value every 5 epochs.

C. Evaluation Metrics

1) Reconstruction quality performance: We use NMSE to evaluate the reconstruction accuracy of the CSI matrix, comparing the original and reconstructed versions, which can be defined as:

$$\text{NMSE} = \mathbb{E}\left[\|\mathbf{H} - \hat{\mathbf{H}}\|_F^2 / \|\mathbf{H}\|_F^2\right], \tag{9}$$

where $\mathbf{H}$ is the original CSI matrix, and $\hat{\mathbf{H}}$ is the reconstructed CSI matrix. Lower NMSE values correspond to higher reconstruction accuracy.

2) Reconstruction Divergence Analysis: We evaluate the effectiveness of the proposed interference detection algorithm by comparing the variance among multiple reconstructed results. To further analyze the quality of the reconstructed results comprehensively, we also calculate the KL divergence (KL) and Wasserstein distance (WD) between the multiple reconstructions. The KL divergence measures the differences in probability distributions among the reconstructed results, while the WD evaluates the geometric alignment consistency of these results. The combined evaluation of these metrics provides a multi-faceted validation of the interference detection algorithm's performance.

TABLE I
THE RECONSTRUCTION PERFORMANCE COMPARISON (IN DB) OF THE PROPOSED AND IMPLEMENTED ALGORITHMS WITH VARYING COMPRESSION RATIOS.

γ	Methods	Indoor	Outdoor	γ	Methods	Indoor	Outdoor
		NMSE	*NMSE*			*NMSE*	*NMSE*
1/4	*CsiNet+*	-44.52	-36.50	1/32	*CsiNet+*	-36.21	-27.84
	CsiNet	-41.37	-34.64		*CsiNet*	-32.08	-27.79
	BCsiNet	-43.46	-35.06		*BCsiNet*	-35.76	-28.19
1/16	*CsiNet+*	-37.68	-29.64	1/64	*CsiNet+*	-33.92	-26.95
	CsiNet	-35.25	-29.19		*CsiNet*	-30.09	-26.90
	BCsiNet	-37.93	-29.58		*BCsiNet*	-32.75	-26.14

Table I presents the NMSE performance of CsiNet, CsiNet+, and the proposed BCsiNet for different compression ratios γ in both indoor and outdoor environments. The results demonstrate that BCsiNet achieves comparable NMSE performance to CsiNet+ while outperforming the traditional CsiNet in reconstruction accuracy. For instance, at a compression ratio of $1/4$, BCsiNet with $\lambda = 0$ achieves an NMSE of -43.46 dB indoors and -35.06 dB outdoors, which closely matches the NMSE values of CsiNet+, i.e., -44.52 dB indoors and -36.50 dB outdoors. In contrast, CsiNet shows lower precision with NMSE values of -41.37 dB indoors and -34.64 dB outdoors.

Table II further provides the divergence metrics, including variance (σ), KL divergence, and Wasserstein distance (WD), for BCsiNet under varying compression ratios γ and interference proportions λ. The results indicate that as λ increases, the divergence metrics consistently increase, reflecting

TABLE II
PERFORMANCE COMPARISON OF VARIANCE, KL DIVERGENCE, AND WASSERSTEIN DISTANCE ACROSS DIFFERENT COMPRESSION RATIOS AND INTERFENCE LEVELS WHEN $\alpha = 0.5$.

γ	*Methods*	**Indoor**			**Outdoor**		
		σ (10^{-4})	*KL* (10^{-5})	*WD* (10^{-7})	σ (10^{-4})	*KL* (10^{-5})	*WD* (10^{-7})
1/4	*BCsiNet (λ=0)*	5.55	1.94	6.29	10.42	3.95	10.97
	BCsiNet (λ=0.2)	8.39	3.32	10.03	12.89	4.84	11.57
	BCsiNet (λ=0.5)	13.07	4.02	13.57	13.12	4.92	11.84
1/16	*BCsiNet (λ=0)*	7.21	3.11	9.25	14.74	5.79	10.39
	BCsiNet (λ=0.2)	8.65	3.73	9.56	16.15	6.42	11.42
	BCsiNet (λ=0.5)	9.50	4.17	10.59	17.12	6.58	11.69
1/32	*BCsiNet (λ=0)*	6.12	2.38	14.62	2.62	0.79	3.45
	BCsiNet (λ=0.2)	6.82	3.34	15.07	4.43	1.66	6.11
	BCsinet (λ=0.5)	7.02	3.45	15.25	4.79	1.87	6.69
1/64	*BCsiNet (λ=0)*	5.88	2.31	5.23	2.62	0.79	3.45
	BCsiNet (λ=0.2)	22.9	10.69	10.23	4.43	1.66	6.11
	BCsiNet (λ=0.5)	24.4	11.17	10.43	4.79	1.87	6.69

higher uncertainty caused by interference. For example, at a compression ratio of $1/4$ in the indoor environment, the KL divergence rises from 1.94 when $\lambda = 0$ to 4.02 when $\lambda = 0.5$, while the Wasserstein distance increases from 6.29×10^{-7} to 13.57×10^{-7}. Similarly, in the outdoor environment, the KL divergence increases from 3.95 to 4.92, and the Wasserstein distance rises from 10.97×10^{-7} to 11.84×10^{-7} as λ grows.

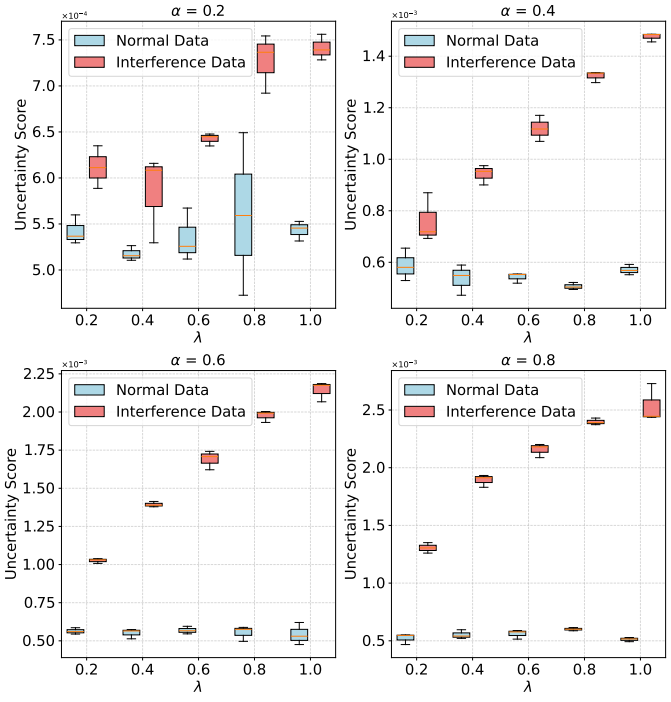

Fig. 1. Uncertainty score comparison between normal and interference data across different α and λ values. Note that adjacent bars in each plot correspond to the same λ value. The plot displays uncertainty scores for both normal data and interference data under five distinct λ settings ($\lambda = 0.2, 0.4, 0.6, 0.8, 1.0$).

Fig. 1 presents the uncertainty scores for normal and noisy data under varying pulse ratios and impulse noise strengths, i.e., α values of 0.2, 0.4, 0.6, and 0.8. Across all subplots, the uncertainty scores for normal data remain consistently low and stable regardless of the pulse ratio, while the noisy data exhibits a clear trend of increasing uncertainty scores as both α and pulse ratio increase. For α = 0.2, the uncertainty scores of noisy data are slightly higher than those of normal data at lower pulse ratios, with a more noticeable increase as the pulse ratio approaches 1.0. When α = 0.4, the uncertainty scores of noisy data become significantly larger compared to normal data, particularly at higher pulse ratios. At α = 0.6, the noisy data shows a further increase in uncertainty scores, with a clear separation from normal data, especially when the pulse ratio exceeds 0.4. For α = 0.8, the uncertainty scores for noisy data reach their highest levels at higher pulse ratios, while the normal data maintains consistently low uncertainty scores across all pulse ratios.

V. CONCLUSION

CSI feedback is essential in wireless communication systems, as it directly impacts key operations such as resource allocation, beamforming, and interference management. Deep learning has shown significant advantages in CSI feedback by automatically extracting complex features, significantly enhancing compression efficiency and reconstruction accuracy. This paper proposes a CSI feedback framework based on BNNs, which achieves high-accuracy CSI reconstruction while effectively detecting potential interference during transmission through uncertainty estimation. Experimental results demonstrate that the proposed method performs well in interference detection under complex transmission conditions, offering a new research direction for improving the robustness and adaptability of CSI feedback. Future work will focus on optimizing detection algorithms to enhance accuracy and efficiency and exploring lossless correction methods after interference detection.

REFERENCES

[1] M. A. Al-Qaness, M. Abd Elaziz, S. Kim, A. A. Ewees, A. A. Abbasi, Y. A. Alhaj, and A. Hawbani, "Channel state information from pure communication to sense and track human motion: A survey," *Sensors*, vol. 19, no. 15, p. 3329, 2019.

[2] F. Li, I. Udoidiok, and J. Zhang, "Reduced-overhead csi feedback for massive mimo through selective component processing," in *2024 IEEE 100th Vehicular Technology Conference (VTC2024-Fall)*. IEEE, 2024, pp. 1–5.

[3] M. H. E. Ali and I. B. Taha, "Channel state information estimation for 5g wireless communication systems: recurrent neural networks approach," *PeerJ Computer Science*, vol. 7, p. e682, 2021.

[4] T. Peken, S. Adiga, R. Tandon, and T. Bose, "Deep learning for svd and hybrid beamforming," *IEEE Transactions on Wireless Communications*, vol. 19, no. 10, pp. 6621–6642, 2020.

[5] J.-C. Shen, J. Zhang, K.-C. Chen, and K. B. Letaief, "High-dimensional csi acquisition in massive mimo: Sparsity-inspired approaches," *IEEE Systems Journal*, vol. 11, no. 1, pp. 32–40, 2016.

[6] C.-K. Wen, W.-T. Shih, and S. Jin, "Deep learning for massive mimo csi feedback," *IEEE Wireless Communications Letters*, vol. 7, no. 5, pp. 748–751, 2018.

[7] J. Guo, C.-K. Wen, S. Jin, and G. Y. Li, "Convolutional neural network-based multiple-rate compressive sensing for massive mimo csi feedback: Design, simulation, and analysis," *IEEE Transactions on Wireless Communications*, vol. 19, no. 4, pp. 2827–2840, 2020.

[8] Z. Liu, L. Zhang, and Z. Ding, "An efficient deep learning framework for low rate massive mimo csi reporting," *IEEE Transactions on Communications*, vol. 68, no. 8, pp. 4761–4772, 2020.

[9] N. Zhao, F. R. Yu, M. Jin, Q. Yan, and V. C. Leung, "Interference alignment and its applications: A survey, research issues, and challenges," *IEEE Communications Surveys & Tutorials*, vol. 18, no. 3, pp. 1779–1803, 2016.

[10] L. Liu, C. Oestges, J. Poutanen, K. Haneda, P. Vainikainen, F. Quitin, F. Tufvesson, and P. De Doncker, "The cost 2100 mimo channel model," *IEEE Wireless Communications*, vol. 19, no. 6, pp. 92–99, 2012.

[11] A. M. Elbir, "A deep learning framework for hybrid beamforming without instantaneous csi feedback," *IEEE Transactions on Vehicular Technology*, vol. 69, no. 10, pp. 11 743–11 755, 2020.

[12] X. Rao and V. K. Lau, "Interference alignment with partial csi feedback in mimo cellular networks," *IEEE Transactions on Signal Processing*, vol. 62, no. 8, pp. 2100–2110, 2014.

[13] A. G. Wilson and P. Izmailov, "Bayesian deep learning and a probabilistic perspective of generalization," *Advances in neural information processing systems*, vol. 33, pp. 4697–4708, 2020.

[14] J. Zhang, F. Li, and F. Ye, "An ensemble-based network intrusion detection scheme with bayesian deep learning," in *ICC 2020-2020 IEEE International Conference on Communications (ICC)*. IEEE, 2020, pp. 1–6.